App. Envi. Res. 39 (2): 1-13

Applied Environmental Research

Journal homepage : http://www.tci-thaijo.org/index.php/aer

Mineralogical and Chemical Characteristics of Gossan Waste Rocks from a Gold Mine in Northeastern Thailand

Thitiphan Assawincharoenkij[1,*], Christoph Hauzenberger[2], Chakkaphan Sutthirat[1,3]

[1] Department of Geology, Faculty of Science, Chulalongkorn University, Bangkok 10330, Thailand
[2] NAWI Graz Geocenter, Petrology and Geochemistry, University of Graz, Universitätsplatz 2, 8010, Graz, Austria
[3] Research Program of Toxic Substance Management in the Mining Industry, Center of Excellence on Hazardous Substance Management (HSM), and Research Unit of Site Remediation on Metals Management from Industry and Mining (Site Rem), Environmental Research Institute, Chulalongkorn University, Bangkok 10330, Thailand
[*] Corresponding author: Email: t.assawincharoenkij@gmail.com; Phone: +662 218 5442

Article History
Submitted: 4 February 2017/ Accepted: 25 March 2017/ Published online: 30 June 2017

Abstract

The mineralogical and chemical compositions of various ocher gossans from a gold mine in northeastern Thailand were investigated, including some heavy metals and other toxic elements. Mineralogical characteristics were carried out using X-Ray Diffractometer (XRD) and Scanning Electron Microscope (SEM) whereas chemical compositions were analyzed using Electron Probe Micro-Analyzer (EPMA). These ocher gossans can be classified, initially based on Munsell color, into five types: type-I (pale-yellow color), type-II (brownish-yellow color), type-III (yellowish-brown color), type-IV (dusky-red color) and type-V (red color). The primary silicate minerals (i.e., quartz, garnet epidote and amphibole) are found in type -I, -II, -III and -IV. They appear to be composed of skarn rock. On the other hand, the secondary minerals (i.e., goethite, jarosite, ankerite, montmorillonite, magnetite, gypsum and secondary quartz) are observed in types-II, -III, -IV and -V. As and Cu are found crucially in types-III, -IV and -V in which both elements can be adsorbed by goethite and/or jarosite. As the result, the gossan rocks in this area are natural adsorbents with high potential to reduce As and Cu contamination into the ecosystem. Therefore, the gossan, a natural attenuation material, is recommended for site remediation because of its low cost and local abundance. Feasibility studies should be conducted to further investigate the potential.

Keywords: Gossan; Adsorption; Toxic Element; Thailand

Introduction

Gossan rocks are commonly associated with massive sulfide ore deposits which have undergone erosion and oxidation processes during uplifting and exposure to the surface [1-5]. Consequently, gossans usually exhibit a mushroom-like morphology [1, 6]. In general, the massive sulfides mainly contain pyrite (FeS_2), pyrrhotite (Fe1-xS), chalcopyrite ($CuFeS_2$) and arsenopyrite (FeAsS) [7-13]. Eq.1-Eq.4 present the oxidation reactions of (Eq.1) pyrite, (Eq.2) pyrrhotite, (Eq.3) chalcopyrite and (Eq.4) arsenopyrite when they react with oxygen and water [2]. The resulting secondary minerals generated include as Fe-oxyhydroxide (goethite: α-FeOOH), hydrous ferric oxide (HFO)), oxides (hematite: Fe_2O_3, magnetite: Fe_3O_4), and oxy-sulfates (schwertmannite: $Fe_8O_8(OH)_6(SO_4)\cdot nH_2O$, jarosite: $KFe_3(SO_4)_2(OH)_6$) [2, 14-18], which are mineral compositions of the gossan rocks [1, 3, 5, 18-20].

The gossan rocks can adsorb toxic elements (including As, Cu, Cd, Fe, Hg, Mn, Pb and Zn) [1, 3, 18, 20] that are possibly released during oxidizing process of the sulfide mining. On the other hand, these toxic elements are naturally attenuated by schwertmannite, K-jarosite and goethite via adsorption and co-precipitation [21]. Therefore, gossan rocks may be useful as attenuation material for site remediation [22].

In Thailand, gold mining activities have raised numerous environmental and health concerns among local communities. The study area is a gold mine in Loei province, northeastern Thailand. Geologically, this area comprises sandstone, siltstone, limestone, granodiorite, skarn, massive sulfide/skarn-sulfide and gossan [7, 20, 23]. The gossan rocks have potential to carry heavy metals/metalloids such as arsenic (up to 810 mg kg^{-1}), copper (up to 7,500 mg kg^{-1}), lead (4−12 mg kg^{-1}) and zinc (45−350 mg kg^{-1}) [20]. They may be classified as ore-bearing or ore-barren gossan rocks [6-7, 24]. The aim of this study was to find out characteristics of various ocher materials including their mineralogical and chemical compositions as well as toxic elements, and also to determine the potential of ocher materials as a natural adsorbent for further study.

$$FeS_{2(s)} + 15/4O_{2(g)} + 7/2H_2O_{(l)} \rightarrow Fe(OH)_{3(s)} + 2SO_{4\,(aq)}^{2-} + 4H_{(aq)}^{+} \quad \text{(Eq.1)}$$

$$Fe_{0.9}S_{(s)} + 2.175O_{2(g)} + 2.35H_2O_{(l)} \rightarrow 0.9Fe(OH)_{3(s)} + SO_{4\,(aq)}^{2-} + 2H_{(aq)}^{+} \quad \text{(Eq.2)}$$

$$CuFeS_{2(s)} + 15/4O_{2(g)} + 7/2H_2O_{(l)} \rightarrow Fe(OH)_{3(s)} + 2SO_{4\,(aq)}^{2-} + Cu_{(aq)}^{2+} + 4H_{(aq)}^{+} \quad \text{(Eq.3)}$$

$$FeAsS_{(s)} + 7/2O_{2(g)} + 4H_2O_{(l)} \rightarrow Fe(OH)_{3(s)} + H_2AsO_{4\,(aq)}^{-} + SO_{4\,(aq)}^{2-} + 3H_{(aq)}^{+} \quad \text{(Eq.4)}$$

Materials and methods

Gossan samples were collected from the waste rock dump site located in a gold mine in the northeastern Thailand (Figure 1). These samples were then classified, initially based on Munsell [25] soil color. Each sample may have different color zones which were selected for laboratory analysis, as shown in Figure 2.

The mineral composition of the samples (types I−V) was determined using a Bruker AXS D8 X-Ray Diffractometer (XRD) based at the NAWI Graz Geocenter, Petrology and Geochemistry, University of Graz, Austria. The operational conditions were set at 40 kV and 40 mA. Micromorphology and texture of the samples were determined by a Scanning Electron Microscope (SEM) (JEOL model LSM-6480LV) at the Faculty of Science, Chulalongkorn University. The operating accelerating voltage was set at 15 kV for capturing images of the samples.

The number of powder samples collected from the gossans was lower than 0.5 g, and thus insufficient for normal analyses by X-Ray Fluo-

rescence (XRF) spectrometry, which re-quires a powder sample of at least 1 g. Therefore, the chemical compositions of these samples were analyzed using a JEOL JXA-8800 Electron Probe Micro-Analyzer (EPMA) at the Depart-ment of Geology, Chulalongkorn University. Each sample was ground (≤ 1 μm) using an agate mortar to homogenize the small amount of sample. These powdered samples were then sprinkled on a carbon tape and then were carbon coated before EPMA analysis. A probe current of 25 nA with a beam spot size of 5 μm were set up with an accelerating voltage of 15 kV for analysis. The detection limit of all elements was 0.05%.

Figure 1 Photographs of mining activities in the study area such as (a) gold processing plant, (b) mining pit showing location of dumped waste rocks of ore-barren gossan in (c, d) the dump sites.

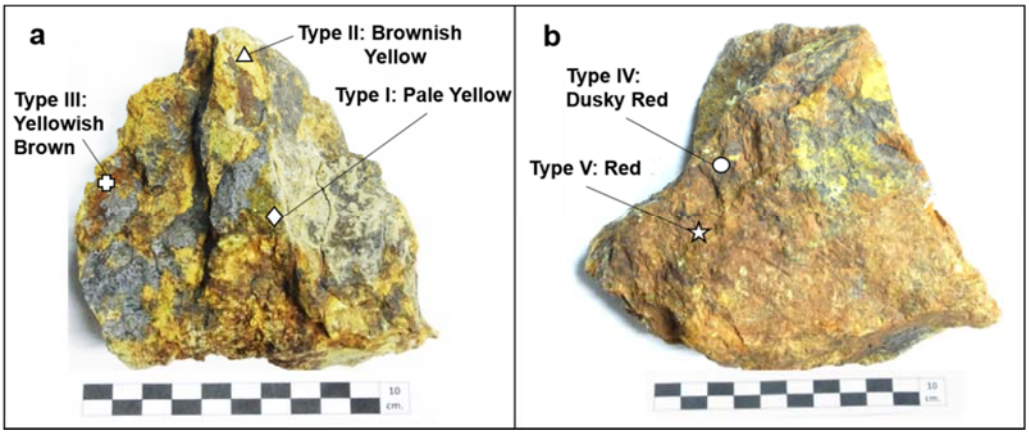

Figure 2 Photographs of gossan rock samples and selected areas for investigation. (a) sample-1 includes type-I: pale yellow, type-II: brownish yellow, and type-III: yellowish brown. (b) sample-2 includes type-IV: dusky red and type-V: red.

Results

1) Mineral texture and assemblage

The ore-barren gossans, dumped as waste rock, were investigated because they contained high levels of toxic elements. These gossans present slightly variable ochre colors ranging from yellow to dark red. These colors are related to the mineral compositions and original rock type. The samples, representatively shown in Figure 2, are classified as type-I (pale yellow color: 5Y 8/4), type-II (brownish yellow color: 10YR 6/8), type-III (yellowish brown color: 10YR 5/8), type-IV (dusky red color: 10R 3/4) and type-V (red color: 10R 4/6). The color codes were allocated following the Munsell (2010) soil color standard.

Micromorphology of types-I and -II present many mineral crystals with an average grain size of 2 to 10 μm (Figures 3a, b); this was clearly confirmed by XRD patterns (Figure 4a, b). They significantly show lath-shaped crystals of primary quartz (Figures 3a, b). On the other hand, types-III, -IV and -V were generally of flaky texture, containing very fine-grained materials of goethite and secondary quartz, with grain size smaller than 1 μm (Figures 3c-e). In addition, different mineral assemblages are also identified using XRD (see Figure 4). Color and mineral assemblage of these sample types are summarized in Table 1. Abbreviations of mineral names were suggested by Whitney and Evans [26].

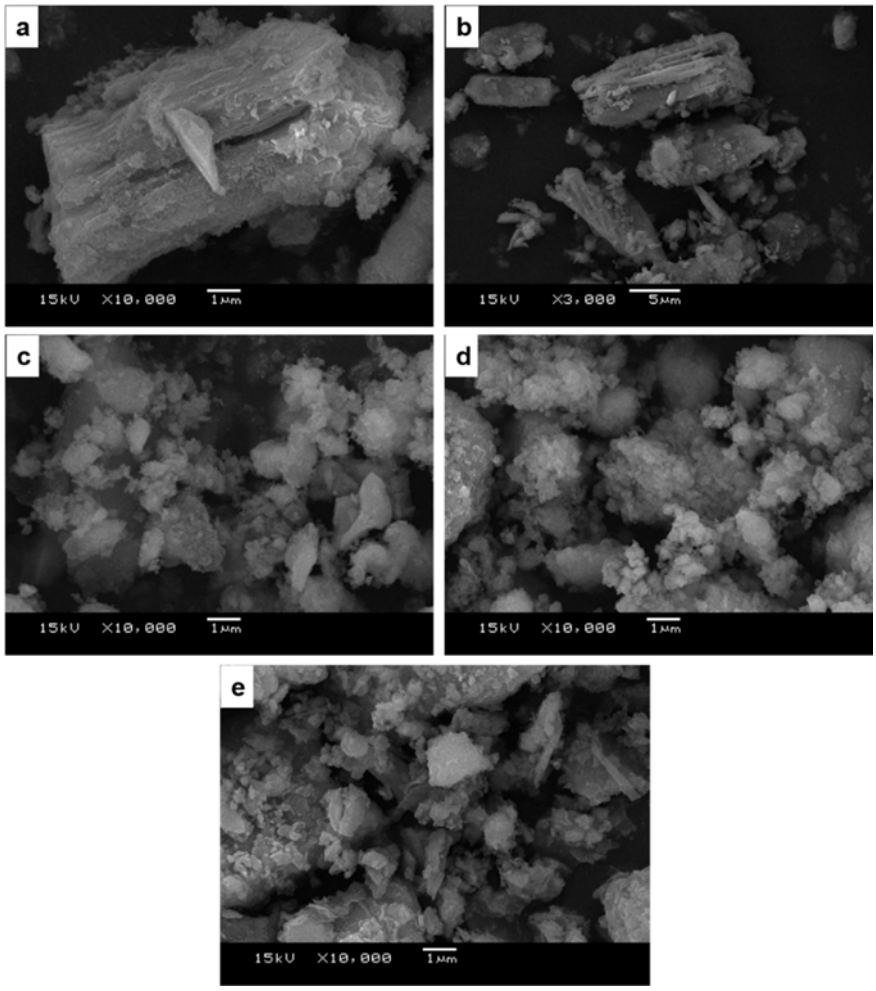

Figure 3 Back Scattering Electron (BSE) images taken from SEM showing micromorphology of: (a) type-I and (b) type-II showing lath-shaped crystals of primary quartz; (c) type-III, (d) type-IV and (e) type-V showing flaky-shaped microcrystalline of goethite and secondary quartz (microcrystalline quartz).

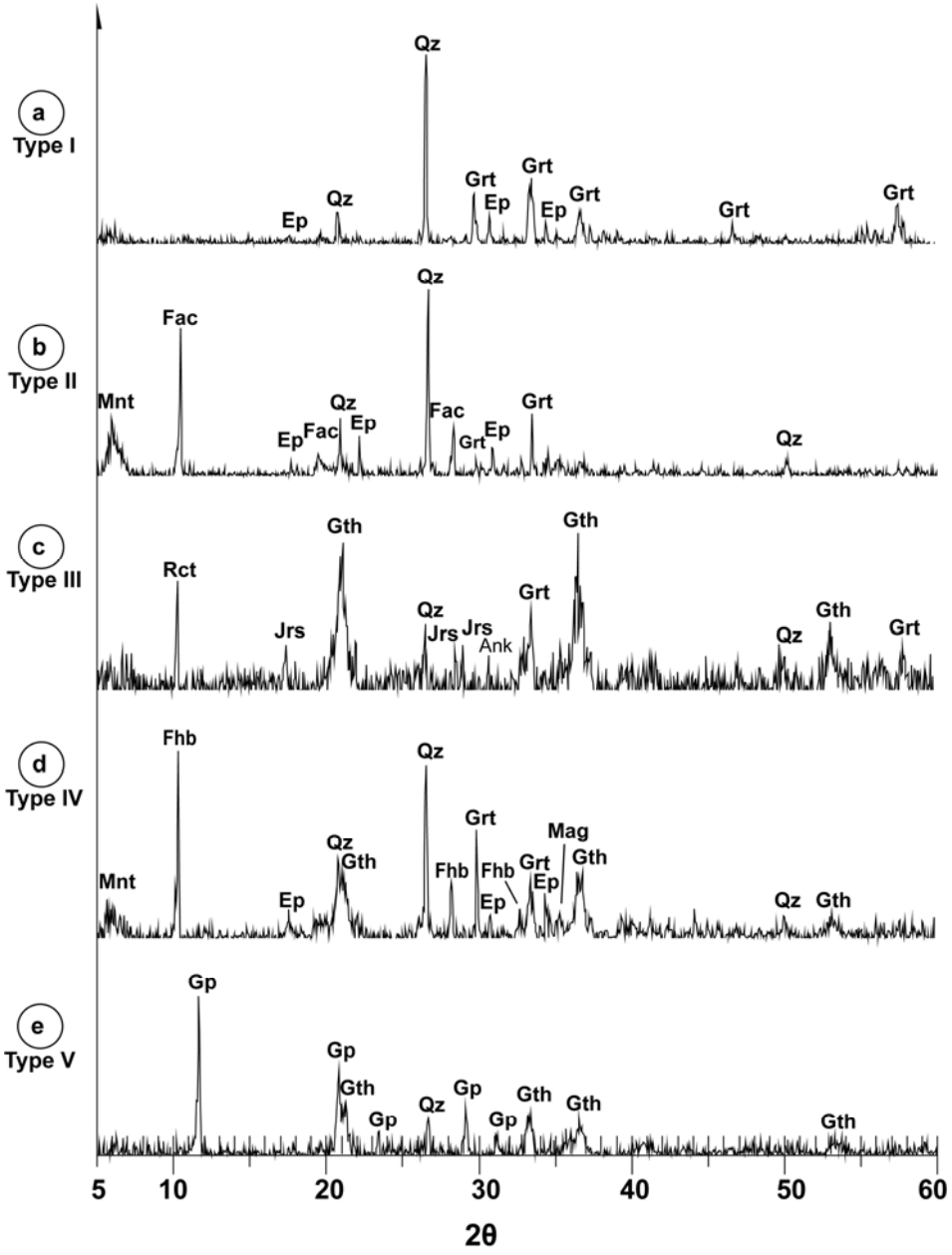

Figure 4 XRD patterns of the samples (a) type-I, (b) type-II, (c) type-III, (d) type-IV and (e) type-V collected selectively from the gossan rocks. Abbreviations of mineral were suggested by Whitney and Evans [26] i.e., Qz (quartz), Ep (epidote), Grt (garnet), Amp (amphibole), Mnt (montmorillonite), Gth (goethite), Jrs (jarosite), Ank (ankerite), Mag (magnetite) and Gp (gypsum).

Table 1 Mineral assemblages and their ideal chemical formula

Sample	Color Munsell*	Mineral assemblage (abbreviation)	Ideal chemical formula
Type-I	Pale Yellow 5Y 8/4	Quartz (Qz)	SiO_2
		Garnet (Grt)	$(Ca_{1.92}Fe_{1.08})Fe_2(SiO_4)_3$
		Epidote (Ep)	$Ca_2(Al_2Fe)(SiO_4)(Si_2O_7)O(OH)$
Type-II	Brownish Yellow 10YR 6/8	Quartz (Qz)	SiO_2
		Garnet (Grt)	$(Ca_{1.92}Fe_{1.08})Fe_2(SiO_4)_3$
		Epidote (Ep)	$Ca_2(Al_2Fe)(SiO_4)(Si_2O_7)O(OH)$
		Amphibole (Amp)	$Ca_2(Mg, Fe, Al)_5(Al, Si)_8O_{22}(OH)_2$
		Montmorillonite (Mnt)	$Na_{0.3}(Al,Mg)_2Si_4O_{10}(OH)_2 \cdot 4H_2O$

Table 1 Mineral assemblages and their ideal chemical formula (*Continued*)

Sample	Color Munsell*	Mineral assemblage (abbreviation)	Ideal chemical formula
Type-III	Yellowish Brown 10YR 5/8	Quartz (Qz)	SiO_2
		Garnet (Grt)	$(Ca_{1.56}Fe_{1.44})Fe_2(SiO_4)_3$
		Goethite (Gth)	FeOOH
		Amphibole (Amp)	$Ca_2(Mg, Fe, Al)_5(Al, Si)_8O_{22}(OH)_2$
		Jarosite (Jrs)	$KFe_3(SO_4)_2(OH)_6$
		Ankerite (Ank)	$Ca_{1.01}Mg_{0.45}Fe_{0.54}(CO_3)_2$
Type-IV	Dusky Red 10R 3/4	Quartz (Qz)	SiO_2
		Garnet (Grt)	$(Ca_{1.56}Fe_{1.44})Fe_2(SiO_4)_3$
		Epidote (Ep)	$Ca_2(Al_2Fe)(SiO_4)(Si_2O_7)O(OH)$
		Amphibole (Amp)	$Ca_2(Mg, Fe, Al)_5(Al, Si)_8O_{22}(OH)_2$
		Goethite (Gth)	FeOOH
		Magnetite (Mag)	Fe_3O_4
		Montmorillonite (Mnt)	$Na_{0.3}(Al,Mg)_2Si_4O_{10}(OH)_2 \cdot 4H_2O$
Type-V	Red 10R 4/6	Quartz (Qz)	SiO_2
		Gypsum (Gp)	$CaSO_4 \cdot 2H_2O$
		Goethite (Gth)	FeOOH

Munsell standard color code* [25]

2) Chemical composition

Table 2 presents qualitative EPMA chemical analyses of the gossan samples. Each sample was analyzed randomly for twenty points. Although this procedure is unconventional for whole-rock analyses, multiple points of analyses with a big beam spot (5 μm) can be statistically representative in a qualitative analysis. This procedure was therefore designed for this study, for which only small amounts of sample were available.

Type-I sample contains 11.28–24.35% Si, 2.11–10.45% Al, 5.32–15.37% Fe, 0.05–1.34% Mg, 0.32–18.83% Ca, ≤ 0.3% Mn, ≤ 0.06% As, 0.05–0.36% Cu and ≤ 0.14% S.

Sample type-II is composed of 10.36–17.72% Si, 1.27–4.05% Al, 16.91–28.01% Fe, 0.47–1.82% Mg, 0.96–2.03% Ca, ≤ 0.26% Mn, ≤ 0.08% Na, ≤ 0.11% As, 0.23–0.60% Cu and ≤ 0.08% S.

Type-III consists of 3.23–11.99% Si, 2.01–5.75% Al, 27.36–40.71% Fe, 0.06–0.31% Mg, 0.20–1.26% Ca, 0.09–2.30% Mn, ≤ 0.06% Na, ≤ 0.21% As, 0.4–0.85% Cu and 0.15–1.75% S.

Type-IV comprised 4.57–8.73% Si, ≤ 2.26% Al, 18.53–21.58% Fe, ≤ 0.35% Mg, 0.08–1.13% Ca, 0.26–4.30% Mn, ≤ 0.05% As, 0.50–0.80% Cu and ≤ 0.43% S.

Type-V sample is mainly comprised of 2.19–17.07% Si, 0.32–1.42% Al, 1.30–16.88% Fe, ≤ 0.27% Mg, 0.49–9.37% Ca, ≤ 0.07% Mn, ≤ 0.05% Na, 0.36–0.57% Cu and 0.35–7.50% S.

Some crucial elements such as Fe, Al, Ca, Mn, S, As and Cu were normalized by Si content and plotted in variation diagrams. Plots of Fe/Si versus other elemental ratios (i.e., Al/Si, Ca/Si, Mn/Si, S/Si, As/Si and Cu/Si) are shown in Figure 5.

In general, all types show similar ratios of Al/Si and Mg/Si ranging commonly between 0.06−0.85 and 0.01−0.15, respectively (Figures 5a, b). Type-I shows clearly high Ca/Si against low Fe/Si (Figure 5c); moreover, it also presents low content of S/Si, As/Si and Cu/Si (see Figures 5d, 5e and 5f). Type-II reveals Ca/Si and As/Si ratios similar to the other types but its Fe/Si, S/Si and Cu/Si ratios are lower than the others except Type I. Type-III is obviously high in Fe/Si and As/Si ratios (Figure 5e) medium ratios of S/Si and Cu/Si (Figures 5d, f). Type-V yields the highest S/Si ratio (Figure 5d). Type-III shows clearly positive correlation between Fe/Si and As/Si (R^2=0.6905). Moreover, all types appear to have positive correlation between Fe/Si and Cu/Si (R^2=0.8608 for Type-III, R^2=0.5542 for Type-IV). According to R-squared value, Fe-ratio has significant relationship with As and Cu. This chemistry results would reflect mineral assemblage and alteration processes of the gossan types, which will be discussed further below.

Table 2 Statistics of EPMA analyses of major and minor elements (Si, Al, Fe, Mg, Ca, Mn and Na), with some crucial trace elements (As, Cu and S) of all types selected from gossan samples, all concentrations in percent weight (%)

	No.	Si	Al	Fe	Mg	Ca	Mn	Na	As	Cu	S
Type-I (n=20)	Min.	11.28	2.11	5.32	0.05	0.32	<0.05	<0.05	<0.05	0.05	<0.05
	Max.	24.35	10.45	15.37	1.34	18.83	0.30	<0.05	0.06	0.36	0.14
	Av.	15.57	5.77	10.35	0.33	6.55	0.12	-	0.02	0.19	0.05
	sd	5.42	3.05	3.40	0.34	6.39	0.09	-	0.03	0.08	0.05
Type-II (n=20)	Min.	10.36	1.27	16.91	0.47	0.96	<0.05	<0.05	<0.05	0.23	<0.05
	Max.	17.72	4.05	28.01	1.82	2.03	0.26	0.08	0.11	0.60	0.08
	Av.	14.47	2.56	23.12	0.92	1.50	0.09	0.05	0.04	0.35	0.03
	sd	2.40	0.87	3.63	0.42	0.39	0.07	0.02	0.03	0.11	0.02
Type-III (n=20)	Min.	3.23	2.01	27.36	0.06	0.20	0.09	<0.05	<0.05	0.40	0.15
	Max.	11.99	5.75	40.71	0.31	1.26	2.30	0.06	0.21	0.85	1.75
	Av.	5.95	2.88	31.46	0.13	0.65	0.72	0.02	0.09	0.58	0.46
	sd	3.15	1.59	6.03	0.07	0.35	0.76	0.02	0.06	0.16	0.44
Type-IV (n=20)	Min.	4.57	<0.05	18.53	<0.05	0.08	0.26	<0.05	<0.05	0.50	0.08
	Max.	8.73	2.26	21.58	0.35	1.13	4.30	<0.05	0.05	0.80	0.43
	Av.	3.34	0.62	10.69	0.11	0.39	1.66	-	0.01	0.49	0.13
	sd	3.11	0.59	7.33	0.10	0.36	1.39	-	0.02	0.19	0.17
Type-V (n=20)	Min.	2.19	0.32	1.30	0.05	0.49	<0.05	<0.05	<0.05	0.36	0.35
	Max.	17.07	1.42	16.88	0.27	9.37	0.07	0.05	<0.05	0.57	7.50
	Av.	7.40	0.67	11.83	0.13	3.30	0.03	0.01	-	0.42	2.62
	sd	4.88	0.36	5.31	0.08	2.41	0.02	0.02	-	0.10	1.96

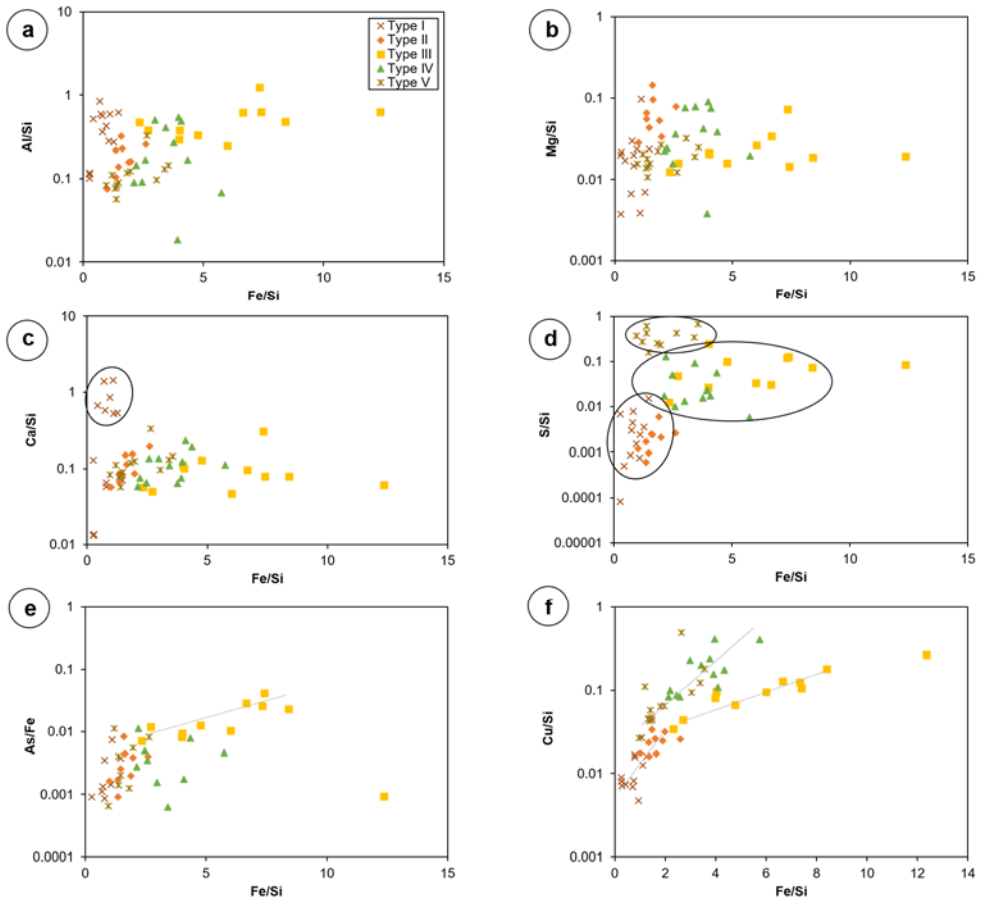

Figure 5 Plots of Fe/Si versus other elemental ratios (Al, Mg, Ca, S, As and Cu against Si).

Discussion

1) Characteristics

In regard to mineral assemblages and chemical composition (e.g., Si, Al, Ca, Mg, Fe and S), all gossan types contain Si as a major element that is compatible to mineral assemblage including quartz (SiO_2) and some other silicate minerals such as garnet $(Ca,Fe)_3Fe_2(SiO_4)_3$, epidote $(Ca_2(Al_2Fe)(SiO_4)(Si_2O_7)O(OH)$, amphibole $(Ca_2(Mg,Fe,Al)_5(Al,Si)_8O_{22}(OH)_2)$ and montmorillonite $(Na(Al,Mg)_2Si_4O_{10}(OH)_2 \cdot 4H_2O)$. Apart from Si, these silicate minerals also contain Al, Ca, Mg and Fe. In addition, Fe is also found associated with the main component of goethite (FeOOH), magnetite (Fe_3O_4) and jarosite ($KFe_3(SO_4)_2(OH)_6$). Sulfur (S) apparently relates to gypsum ($CaSO_4 \cdot 2H_2O$) and jarosite.

Therefore, type-III with the highest iron contents (27−41% Fe) relate clearly to the high amounts of goethite and jarosite present in XRD peak pattern (Figure 4c). Type-V with the highest range of S content (0.35−7.5%) is well fit with the gypsum mainly presented in the XRD peak pattern (Figure 4e).

In general, the XRD analyses also indicate that types-I, -II, -III and -IV consist mainly of primary silicate minerals (i.e., quartz, garnet epidote and amphibole) which appear to be the initial composition of skarn rock. On the other hand, secondary minerals, altered/weathered products (i.e., goethite, jarosite, ankerite, montmorillonite and magnetite), are observed in types-II, -III and -IV. In addition, type-V contain secondary minerals of gypsum, goethite and secondary quartz. Moreover, types-III, -IV and -V that can be easily released under acid conditions could affect the environment to a greater extent than types-I and -II.

For goethite (FeOOH), it may be an oxidation product of sulfide minerals (see Eqs. 1−4) and/or amphibole (see Eq. 5) modified from Velbel [27], or jarosite (see Eq. 6) [28- 29].

According to Eq.5 and Eq.7, quartz (SiO_2) can be produced by amphibole oxidation. Therefore, quartz found in all gossan types can be both primary and secondary minerals which should be confirmed by its micromorphology. Micro-crystalline quartz is mainly present in types-III, -IV and V (Figures 3c-e) which indicate secondary product; on the other hand, gossan types-I and II are composed of primary lath-shaped quartz (Figures 3a, b). These indicate that gossan types-III, -IV and -V may have undertaken more/longer oxidation/ alteration processes than types-I and II.

$$\underset{\textit{Amphibole}}{Ca_2Fe_5Si_8O_{22}(OH)_2} + 4H^+ + 1.25O_2 \rightarrow 2Ca^{2+} + \underset{\textit{Goethite}}{5FeOOH} + \underset{\textit{Quartz}}{8SiO_2} + 0.5H_2O \quad \text{(Eq.5)}$$

$$\underset{\textit{Jarosite}}{KFe_3(SO_4)_2(OH)_6} \rightarrow K^+ + \underset{\textit{Goethite}}{3FeOOH} + 2SO_4^{2-} + 3H^+ \quad \text{(Eq.6)}$$

Type-V consist of quartz, goethite and gypsum which may have weathered from oxidation reaction of amphibole and jarosite (Eq. 7).

$$\underset{\textit{Amphibole}}{Ca_2Fe_5Si_8O_{22}(OH)_2} + \underset{\textit{Jarosite}}{KFe_3(SO_4)_2(OH)_6} + H^+ + 1.5H_2O \rightarrow K^+ + \underset{\textit{Gypsum}}{Ca_2SO_4 \cdot 2H_2O} + \underset{\textit{Goethite}}{8FeOOH} + \underset{\textit{Quartz}}{8SiO_2} + 0.75O_2 \quad \text{(Eq.7)}$$

2) Potential sorption-desorption of toxic element

Based on chemical analyses, type-III has the highest content of Fe, As and Cu. It also shows a positive correlation between Fe and As, Cu (Figures 5e, f); these toxic elements are possibly adsorbed by or co-precipitated with goethite and jarosite [1, 30]. Moreover, types-IV and -V appear to be a source of Cu. The results also indicate a positive trend between Fe and Cu in relation to goethite occurrences because Fe^{3+} in the goethite structure can be substituted by Cu, as suggested by Gerth [31] and Carbone et al. [32].

Adsorption of arsenic and copper onto goethite can be described as a process of surface complexation (≡SOMOH; S=surface, O=oxygen, M=metal and OH=hydroxyl). Surface complexation of arsenic adsorption onto goethite surface is shown in Eq.8 arsenite (As^{3+}) and Eq.9 for arsenate (As^{5+}) as suggested by Kersten and Vlasova [33] and Zhang et al. [34], respectively. In addition, Cu adsorption on goethite is presented in Eq.10 as suggested by Peacock and Sherman [30].

Type-II is a remarkable sample because it consists of As (≤0.11%) and Cu (0.35±0.11%) although it does not consist of goethite or jarosite. In this case, arsenic and copper are possibly adsorbed by montmorillonite (a clay mineral) occurring in this gossan type; this assumption is supported by the study of Lottermoser [2].

Moreover, Assawincharoenkij et al. [20] also suggested that As and Cu may be adsorbed by hydrous ferric oxide (HFO: poor crystalline), usually found as oxidized product along the edges of ferro-silicate minerals, which provide an essential assemblage in type-II. This HFO may transform further to goethite [35].

In addition, particle size highly influences adsorption of toxic elements because smaller particles have a greater reactive surface area, and thus a higher surface adsorption capacity [36]. Therefore, types-III, -IV, and -V, composed of very fine particles < 1 μm, should have higher adsorption potential than types-I and -II (average grain size > 5 μm).

As a result, gossan waste rocks (unwanted rocks) have potential utility as a natural adsorbent material. They consist mainly of goethite (FeOOH), magnetite (Fe_3O_4) and jarosite ($KFe_3(SO_4)_2(OH)_6$) that are recognized as significant natural adsorbents [36-37]. This is supported by prior research into the potential of natural lateritic soil for arsenic adsorption [38-39]. The natural lateritic soils were characterized and potential arsenic adsorbents identified such as goethite, hematite, aluminium hydroxide and kaolinite. Moreover, the natural lateritic soils adsorb the high arsenic content under a wide pH range (from 4.0 to 9.8) as shown by Maiti et al. [38].

$$2(\equiv \mathrm{FeOH})^{-0.5} + \mathrm{As(OH)_3} \leftrightarrow (\equiv (\mathrm{FeO})_2)\mathrm{AsOOH} + 2\mathrm{H_2O} \quad \text{(Eq.8)}$$

$$2(\equiv \mathrm{FeOH}) + \mathrm{AsO_4^{3-}} + \mathrm{H^+} \rightarrow (\equiv (\mathrm{FeO})_2)\mathrm{As(OH)^{-1}} + 2\mathrm{H_2O} \quad \text{(Eq.9)}$$

$$3(\equiv \mathrm{FeOH}) + 2\mathrm{Cu^{2+}} + 3\mathrm{H_2O} \rightarrow (\equiv \mathrm{Fe_3O(OH)_2})\mathrm{Cu_2(OH)_3^0} + 2\mathrm{H^+} \quad \text{(Eq.10)}$$

Figure 6 presents Eh-pH diagram, reported by Majzlan et al. [22], of Fe-oxy hydroxide minerals (i.e., schwertmannite ($(Fe_8O_8(OH)_6(SO_4)\cdot nH_2O$), ferrihydrite ($Fe_5HO_8\cdot 4H_2O$) and green rust ($Fe^{II}$–$Fe^{III}(OH)$); these minerals can adsorb arsenate (As^{5+}) under oxidizing conditions with pH > 2. However, the gossan rocks are unstable under acidic aqueous conditions (pH ≤ 2); Fe-oxyhydroxide can be dissolved, releasing toxic elements into solution [3]. Collected field data of runoff and groundwater should be taken place before experimental design. The crucial information include pH, Eh and toxic elements in these water samples. Subsequently, these gossan waste rocks with proper procedure may be used for site remediation around the gold mine.

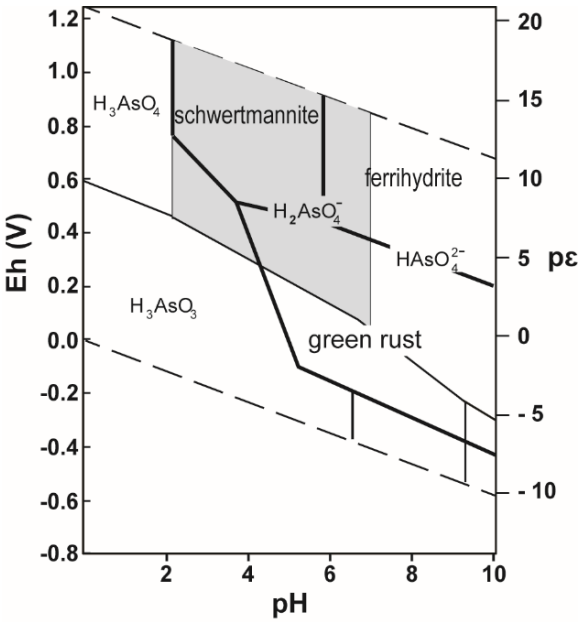

Figure 6 Eh–pH diagram for the systems Fe_2O_3–SO_3–H_2O suggested by Majzlan et al. [40] showing consistency of Fe-oxyhydroxide minerals (i.e., schwertmannite ($(Fe_8O_8(OH)_6(SO_4)\cdot nH_2O$), ferrihydrite ($Fe_5HO_8\cdot 4H_2O$) and green rust ($Fe^{II}$–$Fe^{III}(OH)$) and the speciation of arsenic in the aqueous phase suggested by Majzlan et al. [22].

Conclusion

Gossan waste rocks of various ochre colors were characterized. These different ochre gossans show a relationship between mineral assemblages and chemical composition, including some toxic elements. They can be grouped into five types: type-I, pale-yellow color; type-II, brownish-yellow color; type-III, yellowish-brown color; type-IV, dusky-red color; type-V, red color. Moreover, the gossan rocks including types-III, -IV and -V have a high adsorption capacity and comprised absorbent minerals (goethite, jarosite and montmorillonite), offering potential utility as a natural adsorbent to reduce pollutants (i.e., As and Cu) from the ecosystem. As this rock type (gossan) is abundant around this mining site, it can be recommended for low-cost site remediation.

Acknowledgements

This research project was financially supported by the 90th Anniversary of Chulalongkorn University, Rachadapisek Sompote Fund. The authors would like to thank the Office of Higher Education Commission (OHEC) and the S&T Postgraduate Education and Research Development Office (PERDO) for the support to the Research Program and the Rachadapisek Sompote Endowment Fund, Chulalongkorn University for the support to the Research Unit. Finally, the first author would like to thank the Austrian Federal Ministry of Science, Research and Economy (BMWFW) for ASEA-Uninet/Ernst Mach Grant (Ernst Mach weltweit TSOA) scholarship.

References

[1] Velasco, F., Herrero, J.M., Suárez, S., Yusta, I., Alvaro, A., Tornos, F. Supergene features and evolution of gossans

capping massive sulphide deposits in the Iberian Pyrite Belt. Ore Geology Reviews, 2013, 53, 181-203.

[2] Lottermoser, B.G. Mine Wastes: Characterization, Treatment and Environmental Impacts, 3rd edition. Heidelberg: Springer-Verlag Berlin, 2010, 400.

[3] Romero, A., González, I., Galán, E. Estimation of potential pollution of waste mining dumps at Peña del Hierro (Pyrite Belt, SW Spain) as a base for future mitigation actions. Applied Geochemistry, 2006, 21 (7), 1093-1108.

[4] Smuda, J., Dold, B., Friese, K., Morgenstern, P., Glaesser, W. Mineralogical and geochemical study of element mobility at the sulfide-rich Excelsior waste rock dump from the polymetallic Zn–Pb–(Ag–Bi–Cu) deposit, Cerro de Pasco, Peru. Journal of Geochemical Exploration, 2007, 92 (2-3), 97-110.

[5] Valente, T., Grande, J.A., de la Torre, M.L., Santisteban, M., Cerón, J.C. Mineralogy and environmental relevance of AMD-precipitates from the Tharsis mines, Iberian Pyrite Belt (SW, Spain). Applied Geochemistry, 2013, 39, 11-25.

[6] Assawincharoenkij, T., Hauzenberger, C., Sutthirat, C. Mineralogy and geochemistry of tailings from a gold mine in northeastern Thailand. Human and Ecological Risk Assessment: An International Journal, 2017, 23 (2), 364-387.

[7] Rodmanee, T. Genetic model of Phu Thap Fha gold deposit, Ban Huai Phuk Amphoe Wang Saphung, Changwat Loei. MSc Thesis, Chiang Mai: Chiang Mai University, 2000

[8] Carrillo-Chávez, A., Salas-Megchún, E., Levresse, G., Muñoz-Torres, C., Pérez-Arvizu, O., Gerke, T. Geochemistry and mineralogy of mine-waste material from a "skarn-type" deposit in central Mexico: Modeling geochemical controls of metals in the surface environment. Journal of Geochemical Exploration, 2014, 144 (PA), 28-36.

[9] Koski, R.A., Munk, L., Foster, A.L., Shanks Iii, W.C., Stillings, L.L. Sulfide oxidation and distribution of metals near abandoned copper mines in coastal environments, Prince William Sound, Alaska, USA. Applied Geochemistry, 2008, 23 (2), 227-254.

[10] Álvarez-Valero, A.M., Pérez-López, R., Matos, J., Capitán, M.A., Nieto, J.M., Sáez, R., Delgado, J., Caraballo, M. Potential environmental impact at São Domingos mining district (Iberian Pyrite Belt, SW Iberian Peninsula): Evidence from a chemical and mineralogical characterization. Environmental Geology, 2008, 55 (8), 1797-1809.

[11] Ashley, P.M., Lottermoser, B.G., Collins, A.J., Grant, C.D. Environmental geochemistry of the derelict Webbs Consols mine, New South Wales, Australia. Environmental Geology, 2004, 46 (5), 591-604.

[12] Ferreira da Silva, E., Durães, N., Reis, P., Patinha, C., Matos, J., Costa, M.R. An integrative assessment of environmental degradation of Caveira abandoned mine area (Southern Portugal). Journal of Geochemical Exploration, 2015, 159, 33-47.

[13] Hunt, J., Lottermoser, B.G., Parbhakar-Fox, A., Van Veen, E., Goemann, K. Precious metals in gossanous waste rocks from the Iberian Pyrite Belt. Minerals Engineering, 2016, 87, 45-53.

[14] Campbell, K.M., Nordstrom, D.K. Arsenic Speciation and Sorption in Natural Environments *In:* Bowell, R.J., Alpers, C.N., Jamieson, H.E., Nordstrom, D.K., and Majzlan, J. (eds.), Reviews in Mineralogy and Geochemistry. Chantilly, VA: Mineralogical Society of America, 2014. 185-216.

[15] Lindsay, M.B.J., Moncur, M.C., Bain, J.G., Jambor, J.L., Ptacek, C.J., Blowes, D.W. Geochemical and mineralogical aspects of sulfide mine tailings. Applied Geochemistry, 2015, 57, 157-177.

[16] Lottermoser, B.G. Mine wastes: acidic to circumneutral. Elements, 2011, 7 (6), 393-398.

[17] Anawar, H.M. Sustainable rehabilitation of mining waste and acid mine drainage using geochemistry, mine type, mineralogy, texture, ore extraction and climate knowledge. Journal of Environmental Management, 2015, 158, 111-121.

[18] Atapour, H., Aftabi, A. The geochemistry of gossans associated with Sarcheshmeh porphyry copper deposit, Rafsanjan, Kerman, Iran: Implications for exploration and the environment. Journal of Geochemical Exploration, 2007, 93 (1), 47-65.

[19] West, L., McGown, D.J., Onstott, T.C., Morris, R.V., Suchecki, P., Pratt, L.M. High Lake gossan deposit: An Arctic analogue for ancient Martian surficial processes? Planetary and Space Science, 2009, 57 (11), 1302-1311.

[20] Assawincharoenkij, T., Hauzenberger, C., Ettinger, K., Sutthirat, C. Mineralogical and geochemical characterization of waste-rocks from a gold mine in Northeastern Thailand: Potential source of toxic elements. Environmental Science and Pollution Research *(submitted)*.

[21] Webster, J.G., Swedlund, P.J., Webster, K.S. Trace metal adsorption onto an acid mine drainage iron(III) oxy hydroxy sulfate. Environmental Science & Technology, 1998, 32 (10), 1361-1368.

[22] Majzlan, J., Lalinská, B., Chovan, M., Jurkovič, L.u., Milovská, S., Göttlicher, J. The formation, structure, and ageing of As-rich hydrous ferric oxide at the abandoned Sb deposit Pezinok (Slovakia). Geochimica et Cosmochimica Acta, 2007, 71 (17), 4206-4220.

[23] ERIC The final report: Survey of distribution and sources of heavy metals contamination in Phu Thap Fah Gold Mine Deposit, Khao Luang, Wang Sapung, Loei Province. Bangkok, Thailand (in Thai): Environmental Research Institute, Chulalongkorn University, 2012.

[24] Khon Kaen University Report Final report of Environmental Impact Assessment (EIA). Khon Kaen Province, Thailand (in Thai): Khon Kaen University, 2009.

[25] Munsell, C. Munsell soil color charts: with genuine Munsell color chips. 2010.

[26] Whitney, D.L., Evans, B.W. Abbreviations for names of rock-forming minerals. American Mineralogist, 2010, 95 (1), 185-187.

[27] Velbel, M.A. Weathering of hornblende to ferruginous products by a dissolution-reprecipitation mechanism; petrography and stoichiometry. Clays and Clay Minerals, 1989, 37 (6), 515.

[28] Parbhakar-Fox, A., Lottermoser, B.G. A critical review of acid rock drainage prediction methods and practices. Minerals Engineering, 2015, 82, 107-124.

[29] Grishin, S.I., Bigham, J.M., Tuovinen, O.H. Characterization of Jarosite Formed upon Bacterial Oxidation of Ferrous Sulfate in a Packed-Bed Reactor. Applied and Environmental Microbiology, 1988, 54 (12), 3101-3106.

[30] Peacock, C.L., Sherman, D.M. Copper(II) sorption onto goethite, hematite and lepidocrocite: a surface complexation model based on ab initio molecular geometries and EXAFS spectroscopy. Geochimica et Cosmochimica Acta, 2004, 68 (12), 2623-2637.

[31] Gerth, J. Unit-cell dimensions of pure and trace metal-associated goethites. Geochimica et Cosmochimica Acta, 1990, 54 (2), 363-371.

[32] Carbone, C., Marescotti, P., Lucchetti, G., Martinelli, A., Basso, R., Cauzid, J. Migration of selected elements of environmental concern from unaltered pyrite-rich mineralizations to Fe-rich alteration crusts. Journal of Geochemical Exploration, 2012, 114, 109-117.

[33] Kersten, M., Vlasova, N. Arsenite adsorption on goethite at elevated temperatures. Applied Geochemistry, 2009, 24 (1), 32-43.

[34] Zhang, J.S., Stanforth, R., Pehkonen, S.O. Proton-arsenic adsorption ratios and zeta potential measurements: implications for protonation of hydroxyls on the goethite surface. Journal of Colloid and Interface Science, 2007, 315 (1), 13-20.

[35] Cornell, R.M., Schwertmann, U. The iron oxides: structure, properties, reactions, occurences and uses, 2nd edition. Weinheim: Wiley-VCH Verlag GmbH & Co. KGaA, 2003, 705.

[36] Hua, M., Zhang, S., Pan, B., Zhang, W., Lv, L., Zhang, Q. Heavy metal removal from water/wastewater by nanosized metal oxides: a review. Journal of Hazardous Materials, 2012, 211-212, 317-331.

[37] Asta, M.P., Cama, J., Martinez, M., Gimenez, J. Arsenic removal by goethite and jarosite in acidic conditions and its environmental implications. Journal of Hazardous Materials, 2009, 171 (1-3), 965-972.

[38] Maiti, A., Dasgupta, S., Basu, J., De, S. Adsorption of arsenite using natural laterite as adsorbent. Separation and Purification Technology, 2007, 55 (3), 350-359.

[39] Tongkhan, W., Tantemsaya, N., Thathong, V. Adsorption of arsenic on laterite soil from gold mining area. In Proceeding of the 40th National Graduate Research Conference "Higher Education Hamonization". Prince of Songkla University, Songkla, Thailand, 431-438.